



Full Text View

[Volume 32, Issue 8 \(August 2002\)](#)

Journal of Physical Oceanography

Article: pp. 2361–2378 | [Abstract](#) | [PDF \(663K\)](#)

Inertial Gyre Driven by a Zonal Jet Emerging from the Western Boundary^{*}

Vitalii A. Sheremet

Woods Hole Oceanographic Institution, Woods Hole, Massachusetts

(Manuscript received October 4, 2000, in final form January 14, 2002)

DOI: 10.1175/1520-0485(2002)032<2361:IGDBAZ>2.0.CO;2

ABSTRACT

The problem of a recirculation gyre driven by a zonal jet on a β plane is considered. In a limiting case of a *strong* jet, when the structure of the flow depends only on the momentum flux J of the jet, an asymptotic scaling law for the recirculation gyre is derived: the meridional extent of the gyre depends only on the balance between the inertia of the jet and the opposing β effect, $Y_G = (540J/\beta^2)^{1/5}$, while the zonal extent X_G is linearly proportional to the Reynolds number, Re . Analysis of steady numerical solutions confirms the scaling law. A simplified model of the flow as a combination of a jet carrying a positive momentum flux and a homogenized core of the recirculation gyre carrying an opposite amount of momentum flux provides the quantitative constant in the scaling law, which is in good agreement with the numerical results. Also the gyre is found to form only when the flow in the channel is supercritical with respect to Rossby waves. Thus the recirculation on the β plane can be regarded as a feature similar to a submerged hydraulic jump: a transition between the supercritical flow within the channel and the subcritical (vanishing) flow in the Sverdrup interior of the basin. Laboratory experiments validate the numerical model: there is quantitative agreement with steady solutions and tracer evolution for low Re when flow is close to laminar; for higher Re laboratory experiments show richer behavior, with a strong tendency to asymmetric solutions. Application of the results to the Gulf Stream system is discussed: the meridional scale of the Gulf Stream recirculation $Y_G = 470$ km or 4.2° latitude is predicted, which is consistent with observational data.

Table of Contents:

- [Introduction](#)
- [Jet entering a stagnant](#)
- [Jet-driven inertial gyre:](#)
- [Laboratory experiments](#)
- [Summary and conclusions](#)
- [REFERENCES](#)
- [FIGURES](#)

Options:

- [Create Reference](#)
- [Email this Article](#)
- [Add to MyArchive](#)
- [Search AMS Glossary](#)

Search CrossRef for:

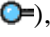
- [Articles Citing This Article](#)

Search Google Scholar for:

- [Vitalii A. Sheremet](#)

1. Introduction

Zonal jets and recirculation gyres are the most dramatic planetary-scale flow features in the ocean: they manifest the interplay between inertia and the β effect. A classical example is the Gulf Stream system. Following the “separation of the

coastline from the Gulf Stream” (as some oceanographers say) near Cape Hatteras, the flow continues straight into the open ocean and between the New England Seamounts and the Grand Banks becomes almost a zonal jet vigorously meandering and shedding rings on both sides. The existence of two large-scale counterrotating gyres north and south of the jet was inferred a long time ago from hydrographic observations (see Figs. 185 and 187 in [Sverdrup et al. 1942](#)). Based on hydrography and a tracer analysis [Worthington \(1976\)](#) presented a quantitative picture for the southern recirculation. A recent compilation of the deep moored long-term current meter data ([Hogg 1992](#)) provided an improved picture ([Fig. 1](#) ) revealing that the recirculations are largely barotropic features with both the northern recirculation gyre and the southern “Worthington gyre” carrying 40–60 Sv each ($\text{Sv} \equiv 10^6 \text{ m}^3 \text{ s}^{-1}$), which should be compared with 30 Sv for the Gulf Stream proper according to the linear wind-driven theory of the subtropical gyre.

Another smaller-scale example is the Alboran gyre in the Western Mediterranean (Alboran Sea), which is driven by the inflow of surface Atlantic waters through the Strait of Gibraltar. This gyre is dramatically seen in infrared satellite imagery ([Preller and Hurlburt 1982](#); [Preller 1986](#); [Lafuente et al. 1998](#)).

Inertial gyres driven by jets may also exist near the ocean bottom. Distribution of potential temperature indicates that colder abyssal flows penetrate from one subbasin into another through numerous fracture zones in the midocean ridges. In the eastern tropical Atlantic, for example, the two most dramatic tongues of colder water originate in the zonally oriented Vema Fracture Zone (11°N) and the Romanche Fracture Zone (near equator) (see Figs. 1 and 2 of [McCartney et al. 1991](#)). Direct velocity measurements in the Vema Fracture Zone ([Polzin et al. 1996](#)) reveal rapid steady currents $O(50 \text{ cm s}^{-1})$ conducive to the formation of inertial gyres at the outlet of the fracture zone. Eastward flow through the Vema Fracture Zone in 1994 was just beginning to carry a low level of chlorofluorocarbons (CFCs; recently introduced into the bottom waters from the atmosphere) acquired in the western Atlantic, and these recently started to enter the Gambia Basin in the bottom water ([Fischer et al. 1996](#)). Therefore, now there is a unique opportunity to document the evolution of deep bottom waters and to detect the existence of such recirculation gyres.

In the context of the wind-driven ocean circulation problem in the subtropical ocean there has been a number of different approaches to explaining the formation of the recirculation gyre. Essentially the western boundary current provides not only the mass transport closure for the interior flow, but also plays an active dynamical role in carrying vorticity and energy poleward. Using a single-layer barotropic model [Kamenkovich \(1966\)](#) gave an explicit solution of the boundary layer equations, revealing the splitting of the current into an inviscid core and a viscous sublayer, and showed that for a finite Reynolds number the boundary layer approximation breaks down due to the onset of the recirculation. This process was further studied by [Ierley \(1987\)](#) using full two-dimensional equations. The fluid parcels within the inviscid core of the boundary current conserve its potential vorticity, but upon reaching the northern end of the basin they obtain negative relative vorticity, preventing their reentry into the Sverdrup interior and thus forming the recirculation. The difficulty in matching the solution in the western boundary layer and in the ocean interior led [Rhines and Young \(1982\)](#) to a theory of recirculation gyres with homogenized potential vorticity, which was confirmed by numerical calculations. A direct action of the wind stress field on the recirculation may result in multiple steady states and inertial runaway, the condition when the recirculation fills the whole basin ([Ierley and Sheremet 1995](#); [Sheremet et al. 1997](#)).

The idea of potential vorticity being advected north by the western boundary current was distilled by [Cessi et al. \(1987\)](#), who proposed a model in which the recirculation is driven by potential vorticity anomalies specified along its boundary. However, a drawback of such a model is that the distribution of the potential vorticity at the boundary, in general, is not known a priori and is a part of the problem: in particular, the zonal extent of the anomalies coincides with the zonal extent of the recirculation.

Another interesting approach was taken by [Marshall and Marshall \(1992\)](#), who analyzed the zonal extent of the recirculation using an inviscid fluid model. At the western boundary they specified the inflow with the prescribed potential vorticity q (functionally dependent on the streamfunction ψ) and let the return flow leave the basin freely also through the western boundary. They found that for $\alpha = dq/d\psi > 0$ [as in the [Fofonoff \(1954\)](#) solution] the recirculation extends all the way to the eastern boundary of the basin, while for $\alpha < 0$ the extent is finite ($\approx 1/\sqrt{|\alpha|}$) and the solution is similar to a modon of [Stern \(1975\)](#). Also a purely inviscid (reduced gravity) model was used by [Nof and Pichevin \(1999\)](#) to analyze the establishment of the Tsugaru and the Alboran gyres. They concluded that the scale of the gyre is determined by the balance between the momentum flux of the inflowing jet and the β effect; however, their approach and results are different from ours.

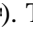
The question of whether the recirculation can be regarded as a secondary flow driven by eddies was addressed by [Holland and Schmitz \(1985\)](#) using a two-layer quasigeostrophic model. Numerical integration showed that momentum from the wind-driven flow concentrated in the upper layer can be transferred to the lower layer by baroclinic perturbations and that recirculations spanning both layers would arise in this way. We note that, if the baroclinic instability is suppressed, then there exists a steady solution in the upper layer only (with the lower layer at rest) identical to the solution of a single-layer barotropic problem. It was also found that the zonal extent of the recirculation is determined by a subtle balance between inertia promoting the penetration of the gyre and eddies trying to reduce its size. A similar viewpoint is adopted in regional

models in which the recirculation is driven by a meandering jet (Jayne et al. 1996; Jayne and Hogg 1999). The jet itself is specified by prescribing inflow (outflow) velocity profiles at the western (eastern) boundaries of the domain. Cummins (1992) studied the emergence of inertial gyres as a result of a nonlinear transfer of energy from eddies to the mean flow; he considered both freely decaying and stochastically forced geostrophic turbulence. Using statistical mechanics, Griffa and Salmon (1989) demonstrated earlier that the inertial gyre on a β plane corresponds to the most probable equilibrium state.

In this paper we take a different approach: we consider a recirculation as a transitional feature between a strong narrow (supercritical) jet and weak or stagnant (subcritical) flow in the Sverdrup interior. Such a viewpoint can be traced back to the work of Rossby (1950), who showed that Rossby waves can have a hydraulic influence—an explanation for the blocking flow patterns in the atmosphere. When the size of the recirculation gyre is large compared to the width of the jet, the velocity profile, distribution of potential vorticity, and total mass flux of the jet become insignificant; in this limit the jet is characterized only by its momentum flux. We also note that by considering a stagnant infinite basin we eliminate the small but complicated interaction between the recirculation gyre and the wind-driven subtropical gyre in the ocean interior.

The structure of the manuscript is as follows: The mathematical formulation of the problem is given in section 2. In section 3 we derive an asymptotic scaling law for the recirculation and compare it with the numerical results. Laboratory experiments, which are used to validate the numerical model, are described in section 4. And finally section 5 summarizes principal results and discusses the implications.

2. Jet entering a stagnant basin on a β plane

Consider a plane jet (flow is independent of depth) emerging from a zonal channel of width $2L$ and entering an infinitely large stagnant basin (see sketch in Fig. 2 ). The origin of the coordinate system is located at the center of the gap in the western boundary (channel opening): x is directed eastward, y northward. We assume that the flow is governed by the two-dimensional Navier–Stokes equations on a β plane:

$$u_t + (uu)_x + (vu)_y + \Pi_x = \nu \nabla^2 u - ru \quad (1)$$

$$v_t + (uv)_x + (vv)_y + \Pi_y + \beta\psi = \nu \nabla^2 v - rv \quad (2)$$

$$\Pi = \frac{p}{\rho} - (f_0 + \beta y)\psi \quad (3)$$

$$u_x + v_y = 0, \quad (4)$$

where u is the zonal and v is the meridional component of velocity, t is time, p is pressure, ρ is the uniform density of the fluid, ψ is the streamfunction, and $u = -\psi_y$, $v = \psi_x$. The subscripts x , y , and t mean differentiation. $\nabla^2 = \partial_x^2 + \partial_y^2$ is the Laplace operator, ν is a kinematic viscosity coefficient. The Coriolis parameter is $f = f_0 + \beta y$. Rayleigh (or bottom) drag (resulting from the Ekman suction at the bottom) with a coefficient r is assumed to be a body force.

Since the flow is two-dimensional, it is convenient to use a streamfunction ψ –vorticity ζ formulation as well, which results from taking the curl of (1) and (2):

$$\zeta_t + J(\psi, \zeta) + \beta\psi_x = \nu \nabla^2 \zeta - r\zeta \quad (5)$$

$$\nabla^2 \psi = \zeta, \quad (6)$$

where $J(\psi, \zeta) = \psi_x \zeta_y - \psi_y \zeta_x$ is the Jacobian operator.

The flow is driven by pumping fluid eastward through the channel at volume rate (per unit depth) $2Q$ and withdrawing it through two sinks of equal strength Q located near the western boundary $x = 0$, $y = \pm\infty$, far north and south of the channel inlet. Mathematically it is equivalent to prescribing the following kinematic conditions: along the southern wall of the channel $x < 0$, $y = -L$ and the southern part of the western boundary $x = 0$, $y < -L$

$$\psi = Q; \quad (7)$$

along the northern wall of the channel $x < 0$, $y = L$ and the northern part of the western boundary $x = 0$, $y > L$

$$\psi = -Q; \quad \text{and} \quad (8)$$

$$\psi = 0 \quad (9)$$

at the eastern boundary $x = +\infty$ which is assumed to be far away eastward. The no-slip condition $u = 0$, $\mathbf{v} = 0$ is specified at all solid walls.

Five parameters characterize the flow: Q , β , ν , r , and the length scale L . Since flow is nondivergent (4), the reference value of the Coriolis parameter f_0 drops out in the streamfunction–vorticity formulation (5), (6): f_0 does not affect velocity fields at all but only modifies the pressure. A wide variety of flow patterns are possible in this problem. We will concentrate our attention on a case when the jet drives two steady and antisymmetric (with respect to the central latitude $y = 0$) inertial gyres with an opposite sense of rotation. This happens (as we shall see) when inertia dominates the friction, which is characterized by the Reynolds number

$$\text{Re} = \frac{Q}{\nu} \gg 1, \quad (10)$$

and when Rossby waves cannot propagate upstream through the channel and perturb the flow there, which corresponds to high Froude–Rossby number

$$\text{Fr} = \frac{\pi^2 Q}{\beta L^3} \gg 1. \quad (11)$$

The fastest long Rossby wave riding on a uniform mean flow $\bar{U} = Q/L$ in a channel of width $2L$ has (group and phase) speed $c = \bar{U} - 4\beta L^2/(m\pi)^2$, where $m = 2$ corresponds to the mode preserving the symmetry of solution. When $\text{Fr} = 1$, this wave is critical (stationary), $c = 0$. Sometimes the nondimensional parameter (11) is called the Rossby number based on β ; however, we adopt the name Froude–Rossby number, as used by [Armi \(1989\)](#), to emphasize the hydraulic analogy.

Within the channel (away from the gap) the flow tends to be zonal with the parabolic velocity profile

$$u = \frac{3Q}{2L} \left[1 - \left(\frac{y}{L} \right)^2 \right] \quad (12)$$

developing when $r = 0$. A more general balance, when $r \neq 0$,

$$\nu u_{yy} - ru = \frac{p_x}{\rho} = \text{const} \quad (13)$$

implies development of a profile that is more uniform near the center with the [Stewartson \(1957\)](#) boundary layers of width $\sqrt{\nu/r}$ forming near the walls.

Assume that the jet drives two recirculation gyres having the meridional extent Y_G (which will be specified later). Far away north and south of the recirculation gyres $|y| \gg Y_G$ the β effect dominates the inertia. The Rossby waves with the meridional scale much larger than Y_G carry the value of streamfunction ($\psi = 0$) from the eastern boundary westward across the Sverdrup interior ($\beta \psi_x = 0$) and press all the currents to the western boundary. Thus a parallel flow will develop with the balance between the β effect and friction [according to (5), (6)]:

$$\beta \psi_x = \nu \psi_{xxxx} - r \psi_{xx}, \quad |y| \rightarrow \infty. \quad (14)$$

The width of the boundary layer is a combination of

$$L_M = \left(\frac{\nu}{\beta} \right)^{1/3}, \quad L_S = \frac{r}{\beta}: \quad (15)$$

the Munk and Stommel layer thicknesses, respectively.

The nonlinear problem (5), (6) was solved numerically using a standard centered-difference approximation with a uniform grid in a finite domain. Besides specifying the conditions (7)–(9), we also specified the gradient conditions for the Poisson equation (6): $\psi_x = 0$ upstream within the channel and $\psi_y = 0$ along the southern and northern limits of the computational domain. Thus we avoided specifying inflow/outflow velocity profiles; instead we let the parallel flow achieve the equilibrium profiles according to (13) and (14). These conditions turned out to be very efficient indeed: it was found that in a steady state away from the recirculation gyres all motions rapidly decay, while in the western boundary layers and within the zonal channel the flow rapidly approaches parallel. Thus the flow enters the domain as a zonal current, drives two counterrotating recirculation gyres, then splits into two equal branches and leaves the domain as two meridional boundary currents.

Time stepping of (5) was performed using a two-layer trapezoid (semi-implicit) scheme (for the nonlinear and β -effect terms), which is symmetric with respect to the present and future time layers. The implicit values of the variables were found by simple iterations. Without dissipation this scheme conserves energy and enstrophy and therefore prevents nonlinear instability. The time integration was started from the irrotational flow $\zeta = 0$ (but u and v are nonzero), which is equivalent to starting pumping impulsively at $t = 0$. The north–south symmetry of the solution was enforced by setting $\zeta(x, -y, t) = -\zeta(x, y, t)$. According to [Ierley and Young \(1991\)](#) the flow in the Munk boundary layer becomes unstable and eddylike perturbations begin to grow for Reynolds numbers larger than $Re_C = 21.574$. To obtain steady solutions for $Re > Re_C$ we introduce an additional term in (5):

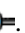
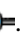
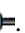
$$\zeta_t = F[\psi, \zeta] - \frac{1}{T_R}(\zeta - \bar{\zeta}^{T_A}), \quad (16)$$



which relaxes the vorticity to a slowly varying time-averaged field

$$\bar{\zeta}^{T_A}(x, y, t) = \frac{1}{T_A} \int_0^\infty \zeta(x, y, t - t') \exp\left(\frac{-t'}{T_A}\right) dt'. \quad (17)$$

The numerical implementation of (17) is $\bar{\zeta}_k^{T_A} = (\tau/T_A)\zeta_{k+1} + (1 - \tau/T_A)\bar{\zeta}_{k-1}^{T_A}$ for $k \gg 1$, where $t = k\tau$; τ is the time step. During the first run without relaxation, the period of the dominant eddy instability is determined, then, in the second run, the averaging time scale T_A is set approximately to that period and the relaxation timescale T_R is typically set equal to T_A in order to suppress the instability. When a steady solution of (16) has been achieved, the time-averaged field (17) becomes identical with the steady one; therefore (16) reduces to $F[\psi, \zeta] = 0$ corresponding to the steady part of (5). This is an inexpensive alternative to Newton's method, allowing one to obtain steady (otherwise unstable) solutions of the nonlinear problem (5), (6). This method works only for moderate supercriticality. Considering steady but unstable flow patterns makes sense because we are focused on the dynamics of the recirculation gyre, which is a more robust feature of the flow. In general, a steady solution of (5), (6) differs from a time-averaged one because of elimination of Reynolds stresses. Also this enables us to understand better the asymptotic behavior of the recirculation gyre for larger Re .

3. Jet-driven inertial gyre: Scaling law

In the absence of the Rayleigh (bottom) drag $r = 0$, the pattern of a steady flow depends only on two nondimensional parameters, Re and Fr . To illustrate the development of the recirculation gyre we present a sequence of steady solutions for $Re = 50$ and increasing Fr in [Fig. 3](#) . The lower half of each plot shows the streamfunction field ψ , while the upper half the potential vorticity $q = \zeta + \beta y$. For slightly supercritical conditions $Fr = 16$ ([Fig. 3a](#) ) the flow just starts to separate from the corner, the recirculation is insignificant, and it cannot be termed an inertial gyre. For larger supercriticality $Fr = 128$ ([Fig. 3b](#) ) the recirculation gyre becomes apparent. The streamfunction maximum at the center of the recirculation is $2.08Q$. The potential vorticity within the core of the gyre tends to be homogenized: the gradients of q within the core are much weaker than the meridional gradient of q outside in the Sverdrup interior. A phenomenon of potential vorticity homogenization within a rapidly rotating gyre was studied by [Rhines and Young \(1982\)](#); it is also applicable more generally to any passive tracer ([Batchelor 1956](#)).

Yet for larger $Fr = 1024$ ([Fig. 3c](#) ) we see further growth of the recirculation gyre in size and in intensity. Note that the zonal extent increases somewhat faster with Fr than the meridional one; therefore the gyre becomes more zonally elongated. The maximum of ψ at the center is $4.49Q$, which is substantially larger than the transport Q of the original jet. The potential vorticity homogenization becomes more dramatic. In [Fig. 4](#)  for the same steady solution we present the meridional sections of the zonal velocity u (solid curve) and the potential vorticity q (dashed curve) at $x = 34.57L$, corresponding to the gyre center. The two plateaus of the homogenized q are clearly visible; they correspond to the cores of the northern and

southern recirculation gyres.

How do dimensions of the recirculation gyre depend on the governing parameters? In order to answer this question we have to bring together several pieces of information. [Schlichting \(1933\)](#); see also [Schlichting 1960](#)) first calculated the flow driven by a round laminar jet using boundary layer approximations. Landau (see p. 89 in [Landau and Lifshitz 1959](#)) presented a solution in spherical coordinates without relying on these approximations. An important result of those works is that the structure of the wake of a *strong* ($Re \gg 1$) jet depends primarily on the momentum flux of the jet rather than on its volume flux. This is due to the fact that the jet entrains the surrounding fluid and its volume transport increases downstream. In the infinitely large fluid the streamlines entering the wake come from infinity (see Fig. 9.14 in [Schlichting 1960](#), chap. IX, sec. g)—no recirculation develops. In a finite domain for large Re recirculation will be limited by the size of the domain.

We note that in the case of a round jet emerging from the wall a recirculation (so-called viscous toroidal eddy) can form for low Re ([Schneider 1985](#); [Zauner 1985](#)). However, the scale of the recirculation grows enormously (exponentially) fast with Re^2 [see [Schneider 1985](#), Eq. (20)]. Therefore this effect can be ignored for large Re .

On a β plane the meridional extent Y_G of the recirculation gyre is controlled by the β effect. To determine Y_G we assume that the advective momentum flux in the recirculation gyre must be of the same order as the advective momentum flux of the jet J (per unit depth and divided by uniform density) within the channel

$$U_G^2 Y_G \simeq J, \quad (18)$$

where U_G is the zonal velocity scale within the gyre. We shall see later that the total momentum flux M consists of the advective flux M_A and the flux due to the pressure (anomaly) M_P . Both M_A and M_P have the same scaling, therefore we use $M_A = J$ in (18). Moreover, we shall see that in our case $M_A + M_P = 0$ in the recirculation gyre. The total momentum flux M reduces from its value J in the channel to zero in the basin because of the negative pressure force acting on the western wall.

Since the potential vorticity tends to be homogenized within the core of the recirculation gyre, the relative vorticity has the same order of magnitude as the planetary

$$\frac{U_G}{Y_G} \simeq \beta Y_G, \quad (19)$$

which can also be interpreted as a hydraulic control: a balance between the mean flow U_G and the speed of Rossby waves βY_G^2 with the meridional scale Y_G . The same result also comes from the y -momentum [equation \(2\)](#) since for the zonally elongated flow the main balance is $\Pi_y = -\beta\psi$.

Thus from (18) and (19) we can express

$$Y_G \simeq \left(\frac{J}{\beta^2} \right)^{1/5}, \quad (20)$$

where the advective momentum flux of the jet

$$J = \int_0^L u^2(y) dy = \frac{6}{5} \frac{Q^2}{L}; \quad (21)$$

the factor 6/5 is for the parabolic velocity profile (12).

The zonal extent of the gyre X_G can be obtained by balancing the zonal advection and meridional diffusion in (1)

$$\frac{U_G^2}{X_G} \simeq \nu \frac{U_G}{Y_G^2}, \quad (22)$$

which becomes more and more accurate for highly elongated gyres at large Re . In other words, X_G is linearly proportional to the *jet* Reynolds number $\text{Re}_J = \text{Re} \sqrt{Y_G/L}$,

$$X_G \simeq Y_G \frac{U_G Y_G}{\nu} \simeq Y_G \frac{\sqrt{J Y_G}}{\nu} = Y_G \text{Re}_J. \quad (23)$$

It should be noted that from a dimensional analysis other length scales can be introduced, such as

$$Y_Q \simeq \left(\frac{Q}{\beta} \right)^{1/3}, \quad (24)$$

which is based on the volume flux of the zonal current within the channel Q rather than on its momentum flux J . This scale may be important for *weak* flows. However, for *strong* jets the scale Y_G according to (20) is more appropriate because the total transport within the recirculation gyre may be several times more than Q . In the limit of Q and $L \rightarrow 0$, while holding J fixed according to (21), the gyre will depend only on J : its transport will be determined by the entrainment process, and the scale Y_Q will be irrelevant.

Similarly, the Rhines scale based on the velocity of the jet U ,

$$Y_U \simeq \left(\frac{U}{\beta} \right)^{1/2}, \quad (25)$$

is not appropriate because U differs from the characteristic velocity within the gyre U_G . Actually, (19) can be regarded as a definition of the Rhines scale based on U_G .

Now that we have established a general scaling law for the gyre, let us develop a more quantitative picture. We deliberately have introduced the “modified” pressure Π so that the x -momentum equation (1) is written down in a conservative form. Integrating (1) along y for fixed x between latitudes where disturbance from the gyre vanishes (due to the symmetry we can use $y = 0$ as the lower limit) and changing the order of integration and differentiation one can get an expression for the change in the zonal momentum flux with x . Integrating it from the eastern boundary, where all motions decay, and expressing the right-hand side in terms of the streamfunction we obtain for the momentum flux M (consisting of an advective part M_A and a part due to pressure M_P)

$$\begin{aligned} M &= M_A + M_P = \int_0^{+\infty} (u^2 + \Pi) dy \\ &= \nu \frac{d}{dx} (\psi(x, +\infty) - \psi(x, 0)) \\ &\quad - r \int_x^{+\infty} (\psi(x', +\infty) - \psi(x', 0)) dx. \end{aligned} \quad (26)$$

The right-hand side contains contributions from the lateral diffusion and bottom drag. Since for large y the streamfunction $\psi(x, +\infty)$ is the solution of the linear boundary layer equation (14), $\psi(x, 0) = 0$ due to the symmetry; therefore the right-hand side in (26) is known, and it is small for small ν and r . In particular, when the lateral friction dominates the bottom drag ($r = 0$), the ratio of the right-hand side to M_A is $(\nu Q/L_M)/(Q^2/L) = O(\text{Re}^{-2/3} \text{Fr}^{-1/3})$ within the boundary layer.

Furthermore, the right-hand side of (26) vanishes outside the western boundary layer because fluid leaves the domain through the western boundary layer and the integrated zonal velocity is zero outside it; $\psi(x, 0) = \psi(x, +\infty) = 0$ for $x \gg (L_M, L_S)$. Thus the meridionally integrated x -momentum flux in the flow is zero at any $x \gg (L_M, L_S)$; $M = M_A + M_P = 0$ and is approximately zero near the western boundary $x = 0$.

At $x = 0$ the advective momentum flux through the inlet is known $M_A = J$ (21) and, apparently, it is approximately balanced (26) by the flux M_P due to the pressure (anomaly) Π (which is negative) acting on the western boundary. As the jet spreads and interacts with the core of the recirculation gyre, both M_A and M_P vary, but the total momentum flux M remains zero.

The modified pressure Π is nonzero only along a part of the western boundary where $|y| < O(Y_G)$. Farther away, where the western boundary current is parallel, $\Pi = 0$ because (1) reduces to $\Pi_x = 0$ and $\Pi = 0$ at infinity. Thus M_P depends on the structure of the flow in the recirculation region. In order to calculate it we will employ a simplified model of the recirculation as a homogenized gyre.

a. Homogenized gyre

Since the potential vorticity q tends to be homogenized, we can use a simplified inviscid flow model (as in Cessi et al. 1987) for the core of the (northern) recirculation gyre:

$$\nabla^2 \psi + \beta y = q_0 = \text{const.} \quad (27)$$

To begin, consider a flow within a rectangle $0 < x < X$, $0 < y < Y$, of small aspect ratio $Y \ll X$, with $\psi = 0$ along the boundary. Near the center of the gyre where the flow is approximately parallel, $\nabla^2 \simeq \partial_y^2$ in (27), therefore the velocity profile and streamfunction are

$$U(y) = u_0 - q_0 y + \frac{1}{2} \beta y^2 \quad (28)$$

$$\Psi(y) = -(u_0 - \frac{1}{2} q_0 y^2 + \frac{1}{6} \beta y^3). \quad (29)$$

The northern boundary is assumed to be a free streamline

$$\Psi(Y) = 0 \quad \text{and} \quad U(Y) = 0, \quad (30)$$

beyond which fluid remains stagnant: $\Psi(y) = 0$, $U(y) = 0$, $\Pi(y) = 0$ for $y \geq Y$. From (30) we obtain

$$u_0 = \frac{1}{6} \beta Y^2 \quad (31)$$

and the homogenized value of the potential vorticity

$$q_0 = \frac{2}{3} \beta Y, \quad (32)$$

while the explicit form of the solution becomes

$$U(y) = \frac{1}{6} \beta (Y^2 - 4Yy + 3y^2) \quad (33)$$

$$\Psi(y) = -\frac{1}{6} \beta y (Y - y)^2. \quad (34)$$

The center of the recirculation ($U(y) = 0$) is located at $y = Y/3$ with the minimum value of the streamfunction

$$\Psi(Y/3) = -\frac{2}{81} \beta Y^3. \quad (35)$$

The “modified” pressure can be calculated from (2), which for the parallel flow reduces to $\Pi_y = -\beta\psi$ and the condition $\Pi(Y) = 0$, meaning that beyond the recirculation gyre flow is stagnant. Thus

$$\begin{aligned}\Pi(y) &= \Pi_0 - \int_0^y \beta\psi \, dy \\ &= \Pi_0 + \frac{1}{12}\beta^2(6Y^2y^2 - 8Yy^3 + 3y^4),\end{aligned}\quad (36)$$

where

$$\Pi_0 = -\frac{1}{72}\beta Y^4;\quad (37)$$

the pressure at the symmetry line between two recirculation gyres is negative. Substituting expressions (33) and (36) into (26) we obtain the total x -momentum flux for the parallel part of the homogenized gyre due to advection and pressure terms (respectively)

$$\begin{aligned}K &= \int_0^Y (u^2 + \Pi) \, dy = \left(\frac{1}{270} - \frac{1}{180}\right)\beta^2 Y^5 \\ &= -\frac{1}{540}\beta^2 Y^5,\end{aligned}\quad (38)$$

which totals to a negative value.

The solution in a whole domain including the inertial layers of width $O(Y)$ near the western and eastern boundaries, where the flow turns around, can be expressed in terms of infinite an Fourier series

$$\begin{aligned}\psi(x, y) &= \Psi(y) - \sum_{m=1,2,3,\dots}^{\infty} \hat{\Psi}_m \sin\left(\frac{m\pi y}{Y}\right) \\ &\quad \times \left[\exp\left(-\frac{m\pi x}{Y}\right) + \exp\left(-\frac{m\pi(X-x)}{Y}\right) \right],\end{aligned}\quad (39)$$

where it is assumed that two exponential tails do not overlap, $Y \ll X$ (otherwise one has to consider hyperbolic cosines):

$$\begin{aligned}\hat{\Psi}_m &= -\frac{2}{3} \frac{\beta Y^2}{(m\pi)^3} C_m, & C_m &= 1 & \text{if } m \text{ is odd,} \\ & & C_m &= -3 & \text{if } m \text{ is even}\end{aligned}\quad (40)$$

are the Fourier coefficients of (39).

The total x -momentum flux K must be the same at any x in the homogenized gyre including the western and eastern boundaries. This can be checked independently if we recall the Bernoulli equation

$$\frac{(u^2 + v^2)}{2} + p = \text{const}[\psi];\quad (41)$$

in an ideal fluid the Bernoulli function is a constant along a streamline. For the streamline $\psi = 0$ bounding the gyre we

have, for example along the western boundary ($x = 0, u = 0$), $\Pi = p = -v^2/2$ and, hence, the total momentum flux at the boundary has a contribution only from the pressure

$$K_0 = \int_0^Y \Pi \, dy = - \int_0^Y \frac{v^2}{2} \, dy. \quad (42)$$

Substituting (39) and (40) into (42) and using the orthogonality of the basis functions gives momentum flux

$$\begin{aligned} K_0 &= -\frac{\pi^2}{4} Y \sum_{m=1,2,3,\dots}^{\infty} \hat{\Psi}_m^2 m^2 \\ &= -\frac{\beta^2 Y^5}{9\pi^4} \sum_m C_m^2 \frac{1}{m^4}. \end{aligned} \quad (43)$$

Summing up odd and even terms separately and using



$$\sum_{k=1,2,3,\dots}^{\infty} \frac{1}{(2k-1)^4} = \frac{(2^4-1)\pi^4}{24!} |B_4| = \frac{\pi^4}{96} \quad (44)$$

$$\sum_{k=1,2,3,\dots}^{\infty} \frac{1}{k^4} = \frac{2^2\pi^4}{4!} |B_4| = \frac{\pi^4}{180} \quad (45)$$

from [Gradsteyn and Ryzhik \(1980, p. 7, formulas 0.233.5 and 0.233.3\)](#), where $B_4 = -1/30$ is one of the Bernoulli numbers, we arrive at the same value as in (38):

$$K_0 = -\frac{1}{540} \beta^2 Y^5 = K, \quad (46)$$

which confirms our algebraic manipulations.

The homogenized gyre like (39) cannot exist without solid walls at the western and eastern boundaries, which exert forces on the flow due to the negative pressure anomalies and provide sources and sinks of the x -momentum flux. However, we can think of the recirculation gyre system in its western part as a combination of the jet emerging from the western boundary, carrying positive advective momentum flux J and the core of the recirculation gyre carrying the negative total momentum flux K . [The profiles of u (dash-dotted line) and q (dotted line) according to the homogenized core model (33), (32) are shown in [Fig. 4](#) ]. The meridional scale Y_G according to (47) is marked by vertical lines.] As we move eastward toward the center of the gyre and farther, the jet spreads due to diffusion and interacts with the core of the gyre, the profile of the zonal velocity u adjusts to a new smoother state (the actual profile near the center of the gyre; see the solid curve in [Fig. 4](#) ) and the momentum fluxes combine. The flow as a whole can have a finite eastward extent without the necessity of the eastern solid wall if the total momentum flux $M = J + K = 0$.

As has been already mentioned, at the western boundary ($x = 0$) the advective part of the momentum flux is associated with the entering jet, $M_A = J$, while the momentum flux due to the pressure anomaly force Π (which is negative) acting on the western boundary is identified with the momentum flux of the homogenized gyre, $M_p = K_0 = K$. We can distinguish between the force on the solid wall, which involves the integral from L to infinity, and M_p , which involves the integral from zero to infinity. For narrow jets, $L \ll Y_G$, the difference is negligible. Thus from this simplified model, balancing J and K and combining (38) and (21), we obtain a quantitative prediction for the meridional scale of the recirculation gyre


$$Y_G = \left(\frac{540J}{\beta^2} \right)^{1/5}. \quad (47)$$


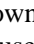

Obtaining a quantitative result for X_G is much more difficult: it requires numerical solution of the advection–diffusion equation. Possibly, some progress can be achieved using a boundary layer approximation for elongated gyres ($Y \ll X$).


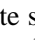
To compare the theoretical prediction with the numerical solution of the fully nonlinear problem, we rewrite the scaling law (47), (23) in a nondimensional form in terms of Fr and Re for the channel

$$\frac{Y_G}{L} = \left(\frac{648}{\pi^4} \right)^{1/5} (\text{Fr}^{2/5} - 1) \quad (48)$$

$$\frac{X_G}{L} \simeq \text{Fr}^{3/5} \text{Re}. \quad (49)$$

As with any asymptotic formula there is an uncertainty at the origin; therefore, we added -1 as the last term in (48) to match the numerical data. We will discuss this below. To make a quantitative check we define the zonal extent of the gyre X_G as a distance from the channel opening to the first stagnation point $u(X_G, 0) = 0$ along the symmetry line $y = 0$. To be consistent with (30), the meridional extent Y_G is defined as the latitude of the zero streamline $\psi(X_C, Y_G) = 0$ near the center of the gyre X_C . The measure Y_G is not very sensitive to the exact location in x because the flow is fairly parallel near the center of the gyre for large Fr. However, for $Y_G < 4$ this measure becomes ambiguous because no quasi-parallel flow can be identified (see Fig. 3a ) and the recirculation cannot be termed as an inertial gyre.

The meridional extent of the gyre Y_G is shown in Fig. 5a ) as a function of $\text{Fr}^{2/5}$ over a wide range of Fr for several fixed values of $\text{Re} = 20, 50, 100, 200$. (Only the cases with a “healthy, mature” gyre for which Y_G is measured without ambiguity are shown. For example, the case shown in Fig. 3a ) does not contribute a datum to Fig. 5a ) The solutions for $\text{Re} = 20$ were stable, while for larger Re we used the stabilization method (16), (17) to get to a steady state. It is clear that the data for different Re tend to lie along a straight line and converge as Re is increased. This validates the factor $2/5$ in the scaling law. The agreement with the formula (48) shown by a straight solid line is excellent. The addition of the term -1 in (48) does not change the asymptotic behavior at large Fr, but it makes perfect sense in terms of the hydraulic interpretation: the size of the recirculation gyre depends on the supercriticality, and the recirculation gyre tends to disappear at the critical Froude–Rossby number $\text{Fr} = 1$. We stress once again that the meridional extent Y_G is independent of Re and is only determined by the balance between inertia and the β effect, which validates the momentum flux arguments given above.

We plotted the zonal extent of the gyre X_G divided by $L\text{Re}$ as a function of $\text{Fr}^{3/5}$ in Fig. 5b ) . As expected, all the data tend to lie along straight lines when the gyre is large, $\text{Fr} \gg 1$, which confirms the scaling (49). For the case of $\text{Re} = 20$, the viscous effects are significant and the gyre itself is not much larger than L ; therefore, the line corresponding to $\text{Re} = 20$ is slightly displaced relative to those for higher Re. The cases $\text{Re} = 50, 100$ and 200 match each other much better. The quantitative coefficient in the scaling formula (49) or the slope in Fig. 5b ) is quite small, specifically 0.033 for $\text{Re} = 20$, 0.029 for $\text{Re} = 50$, and 0.027 for $\text{Re} = 100$ and 200 . This is consistent with other problems where the length of the recirculation increases linearly with the Reynolds number. For example, for a laminar flow past a circular cylinder such coefficient is also small, 0.06 (Taneda 1956). It is clear that the gyre develops only for large Fr, when the jet is supercritical. As the criticality condition is approached $\text{Fr} = O(1)$, near the origin of the plot, the gyre becomes comparable with L or with the Munk thickness L_M (whichever is greater) and tends to disappear, the scaling law breaks down, and the curve deviates from the straight line.


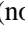
Drawing an analogy to other hydraulic problems, we can say that the recirculation gyre on a β plane is a region of transition from the supercritical flow in the narrow part of the channel to the subcritical flow in the Sverdrup interior. The compact inertial gyre can only form in the presence of the β effect (without β the inertial recirculation will grow to fill the whole basin), and it forms when the flow in the inlet is supercritical (otherwise the Rossby wave will propagate into the channel and change the velocity profile upstream). It is a feature similar to a *submerged* hydraulic jump, as in the case of a drowned outflow from a sluice gate (see Henderson 1966, Fig. 6-24 on p. 208). The meridional scale of the gyre Y_G depends on the *supercriticality* of the flow, $\text{Fr}^{2/5} - 1$, expressed in terms of the Froude–Rossby number Fr, similar to the way the amplitude of the hydraulic jump depends on the supercriticality $\frac{1}{2}(\sqrt{1 + 8F_1^2} - 1)$ [Chow 1959, Eq. (3-21)] expressed in terms of the classical Froude number F_1 . In this respect L is analogous to the clearance of the sluice gate while Y_G is analogous to the fluid depth behind the jump. We emphasize the analogy to the *drowned* outflow because in both cases the pressure forces on the wall are important in determining the structure of the recirculating flow. Furthermore, the zonal scale of the gyre is similar to the length of the “roller” or a region of recirculating turbulent flow. It depends on the strength of turbulent dissipation, which in turn is determined by the strength of the jump. As illustrated by Chow (1959, Fig. 15-4 on p. 398), the ratio of the length of the roller to the height of the jump saturates at about 6 for large Froude numbers. We have to realize that the viscosity ν in our laminar case is a gross parameterization of the turbulent diffusion.

We mention that the slightly different power factor of $1/3$ is often used to rationalize observed dependence of the meridional size of recirculation on Froude–Rossby number (translating into dependence on $\beta^{-1/3}$). Essentially, this stems from the assumption that the meridional scale of the gyre is determined by the total volume flux of the jet as in (24) rather than by its momentum flux as in (20). For example, [Jayne et al. \(1996\)](#) (see also [Jayne and Hogg 1999](#)) in the theory of recirculation driven by an unstable jet use a condition that “the normalized jet transport equal that prescribed at the inlet.” As already mentioned, the total volume flux is not an appropriate quantity due to entrainment of the ambient fluid by the jet: the total transport of the gyre may be significantly larger than the volume flux of the jet at the inlet.

We note that $2/5$ and $1/3$ are actually very close and it is difficult to distinguish between them based on Y_G ranging roughly from 4 to 20 in our numerical experiments. However, plotting the Y_G data versus $\text{Fr}^{1/3}$ would produce small but noticeable upward curvature. Thus, the excellent agreement between the numerical data and the theoretical dependence (48) and also the physical arguments, that it is the momentum flux J rather than the volume transport Q of the jet being the appropriate parameter, allow us to speak in favor of the factor $2/5$ over $1/3$.

b. Effect of bottom drag

As known from previous studies, for example, [Ierley and Sheremet \(1995\)](#), the lateral friction and bottom drag dissipation mechanisms can produce significantly different steady circulation patterns. Lateral friction has a selective effect on motions of small spatial scales; therefore, for large Reynolds numbers we were able to neglect it in the core of the recirculation gyre. In contrast, bottom drag acts uniformly on all spatial scales, causing relative vorticity to decay exponentially with the spinup (-down) time $T_S = 1/r$. This should result in a general decrease of velocities throughout the recirculation gyre.

In order to illustrate the effect of bottom drag we obtained numerical solutions for $\text{Re} = 50$, $\text{Fr} = 1024$ and increasing r . (We do not present these solutions in the paper, but qualitatively similar solutions for $\text{Re} = 6.5$, 13, and 26 will be shown and discussed in the next section; the case with $r = 0$ was shown in [Fig. 3c](#) ) Based on these steady solutions we plot in [Fig. 6](#)  several measures of the recirculation gyre scales as functions of r (nondimensionalized by the advective time scale in the channel L^2/Q). The measures X_G and Y_G are the same as introduced before for the cases with $r = 0$; they are based on the configuration of the streamline $\psi = 0$. The problem with these measures for finite r is that the decay of the streamfunction in the far field ceases to be oscillatory, therefore the isoline $\psi = 0$ retreats to infinity, thus failing to be a proxy for the recirculation gyre boundary.

It appears that the transition from oscillatory to nonoscillatory decay is correlated with the structure of the western boundary current outside of the recirculation gyre, which is determined by the relative thicknesses of the Munk L_M and Stommel L_S boundary layer (15). Substituting $\psi \simeq \exp(\lambda x)$ into (14) gives a cubic characteristic equation

$$\lambda^3 + p\lambda + q = 0, \quad \text{where } p = -\frac{L_S}{L_M^3},$$

$$q = -\frac{1}{L_M^3}. \quad (50)$$

The number of real roots of this equation depends on the value of the discriminant

$$D = \left(\frac{p}{3}\right)^3 + \left(\frac{q}{2}\right)^2 = \frac{1}{L_M^6} \left(-\frac{1}{3^3} \left(\frac{L_S}{L_M}\right)^3 + \frac{1}{2^2} \right). \quad (51)$$

When the lateral friction dominates, for $L_S/L_M < 3 \times 2^{-2/3} = 1.8899$, $D < 0$, there are one real and two complex conjugate roots. The behavior of ψ is oscillatory for large x as in the Munk boundary layer, with the zones of forward and reversed current. When the bottom drag dominates, $L_S/L_M > 1.8899$, $D > 0$, all roots are real, the decay is monotonic as in the Stommel boundary layer, and $\psi = 0$ is attained at infinity. In a nondimensional form the condition $D = 0$ translates into

$$\frac{\text{r}}{(Q/L^2)} = 3 \times 2^{-2/3} \left(\frac{\text{Fr}}{\pi^2}\right)^{-2/3} \text{Re}^{-1/3}, \quad (52)$$

which for $Re = 50$ and $Fr = 1024$ equals 0.0232 . This value is marked in [Fig. 6](#) by a vertical line and a symbol r_0 . As r increases and approaches r_0 , the two measures X_G and Y_G diverge. Even for r substantially smaller than r_0 the measure Y_G may be ambiguous because the gyre lacks the region of quasi-parallel flow (see [Figs. 8](#), [9b](#), and [11c](#)).

We also plot in [Fig. 6](#) other scales of the gyre. The measure $X_G[\zeta = 0]$ is similar to X_G , but is based on the relative vorticity field. It is defined as the distance along $y = 0$ from the channel opening to the first zero of ζ . The measure Y_R is the distance from the symmetry line $y = 0$ to the point of reattachment of the isoline $\psi = Q$ to the western boundary $x = 0$. The maximum value of the streamfunction at the center of the gyre Ψ_G is multiplied by a factor of 10 to appear in the same plot. All curves are represented by different line styles and are clearly labeled.

It is seen that, as the bottom drag increases, it is the transport of the gyre that decreases most rapidly from $\Psi_G = 4.49Q$ for $r = 0$ to a value slightly above Q . Substantial decrease of the zonal scales of the gyre X_G and $X_G[\zeta = 0]$ occur for larger r . It appears that the least susceptible to bottom drag are the meridional scales of the gyre Y_G and Y_R : Y_G even increases and diverges as $r \rightarrow r_0$; at this stage, however, Y_G is not a characteristic scale of the recirculation. From the scale analysis it follows that bottom drag should be an important factor in the dynamics of the recirculation gyre if the spindown time $T_S = 1/r$ is comparable with the characteristic time scale of fluid parcel motion in the gyre $T_G \cong X_G Y_G / \Psi_G$. Taking the values $X_G = 87.5L$, $Y_G = 21.7L$, $\Psi_G = 4.49Q$ for $Re = 50$, $Fr = 1024$, and $r = 0$ we get $r/(Q/L^2) = 0.00236$, which is consistent with the decay scale of Ψ_G in [Fig. 6](#).

4. Laboratory experiments and comparison with numerical solutions

To validate the results of the numerical model we conducted a series of relevant laboratory experiments on a rotating platform. The experimental design is shown in [Fig. 7](#). The rectangular tank made of acrylic had inner horizontal dimensions $61 \text{ cm} \times 61 \text{ cm}$ and a bottom with slope $s = dz/dy = -0.1$ to model the β effect

$$\beta = \frac{fs}{H}. \quad (53)$$

In the experiments reported, the platform was rotated anticyclonically at $f = -2 \text{ s}^{-1}$, as if we were in the Southern Hemisphere, to produce positive β and westward propagation of Rossby waves. Water was entering the basin $40 \text{ cm} \times 61 \text{ cm}$ in x and y , respectively, through a narrow vertical channel of width $2L = 0.5 \text{ cm}$. It was withdrawn at two sinks located in the southwestern and northwestern corners of the basin. Each sink consisted of a circular aluminum pipe 48 mm in diameter with a narrow (1 mm) vertical side slit to make vertically uniform flow. Two constant displacement pumps delivered equal flow rates to achieve symmetry. Before entering the zonal channel, the fluid was collected in a small flume-shaped reservoir in order to damp the turbulence and produce a vertically uniform flow. The pumping system was closed so that the fluid level in the basin remained practically the same: $H = 5 \text{ cm}$ at the central latitude. Essentially, the flow was controlled by surface gravity waves at the *narrows* of the inlet channel and the sinks; therefore, small level changes during the transient periods theoretically existed, but they were negligibly small. The top of the tank had a transparent cover to shield the free surface of the fluid from air friction and evaporation.

It was bitterly discovered that due to internal heat generation within the pumps (Cole–Palmer Model 7617-70) the temperature of the water changed by about $\Delta T \cong 0.5^\circ\text{--}1^\circ\text{C}$ upon going through the pump during typical conditions. To eliminate resulting buoyancy effects, especially important at slow flow rates, the water leaving the pumps was collected in a rubber bladder immersed in a closed jar. As the bladder expanded, it was displacing the water originally present in the jar having the same temperature T_0 as in the experimental tank. Therefore the duration of the experiment was limited by the volume of the jar, typically to about 30 min. The tank was insulated and the jar was placed in a water bath.

The change of fluid depth in the tank from one side to another was finite, therefore the quasi-geostrophic [equations \(5\), \(6\)](#) would be invalid for the basin-scale flows; however, for the much smaller recirculation gyres the quasigeostrophic approximation is appropriate. Within the narrow inlet channel the Rossby number was not small, but it was observed that the flow was two-dimensional anyway due to other factors.

As with most laboratory experiments the bottom drag due to the suction in the bottom Ekman boundary layer is a significant effect compared with the lateral friction; therefore, we cannot check the theoretical predictions for $r = 0$ directly. The e -folding spinup timescale was

$$T_S = \frac{1}{r} = 50 \text{ s}, \quad (54)$$

where

$$r = \frac{fh_E}{2H}, \quad h_E = \sqrt{\frac{2\nu}{f}}. \quad (55)$$

For comparison with the laboratory experiments we solved (5) numerically taking into account the Rayleigh drag coefficient r . The flow was visualized by introducing occasionally a small amount of dye to the water in the reservoir upstream of the channel, which mixed rapidly due to turbulence there. Ideally, during a steady flow the dyed water would be restricted to the area within the streamline $\psi = 0$ if we neglect the diffusivity of the dye (which is about a thousand times smaller than the diffusivity of momentum). After initial spinup had been completed and fluid reached a solid body rotation, pumps were switched on and dye introduced. The dyed fluid started to enter the basin, while the flow was equilibrating to a new state.

To validate the numerical model we consider three laboratory experiments with increasing flow rate (per unit depth) Q (other parameters being fixed: $L = 2.5 \text{ mm}$, $H = 5.0 \text{ cm}$, $f = 2.00 \text{ s}^{-1}$, $\nu = 1.00 \times 10^{-2} \text{ cm}^2 \text{ s}^{-1}$ at $T = 20^\circ\text{C}$), hence increasing both Re and Fr.

In the experiment with $Q = 6.5 \times 10^{-2} \text{ cm}^2 \text{ s}^{-1}$ (corresponding nondimensional parameters $\text{Re} = 6.5$, $\text{Fr} = 1026$, $T_S Q/L^2 = 52$) the flow reaches a laminar steady state. The photograph of the dye distribution at the moment when the gyre has attained an equilibrium size is shown in Fig. 8 with several streamlines of a corresponding steady numerical solution superimposed. We see good agreement in terms of the shape and extent of the recirculation gyre. The motion and pattern of dye distribution within the recirculation gyre stabilizes first, while the distribution of dye in the western boundary layer has not reached an equilibrium yet. In the northern boundary layer the most advanced portion of dyed fluid has a shape similar to the head of a gravity current. Some asymmetry in the amount of dyed water spreading in the northern and southern boundary layers is also noticeable in Fig. 8.

For larger $Q = 13 \times 10^{-2} \text{ cm}^2 \text{ s}^{-1}$ ($\text{Re} = 13$, $\text{Fr} = 2053$, $T_S Q/L^2 = 104$) the flow has a mild degree of time dependence: the jet develops sinuous instability immediately near the inlet (Fig. 9a). The periodic flow perturbations decay farther downstream, closer to the edge of the gyre, but the dye pattern gets stretched by shear near the stagnation point resulting in a formation of long filaments of dyed fluid. During the initial growth the southern and northern gyres appear to be symmetrical. Figure 9a shows a stage at which the extent of the recirculation is somewhat shorter than its limiting value. Unfortunately, as time marches on, flow tends to a quasi-steady asymmetric state in which one of the gyres dominates the other (Fig. 9b). Preference of a particular asymmetric state depends on initial perturbations of velocity (and buoyancy if any) and, during the course of an experiment, flow may spontaneously flip between two asymmetric states.

Such behavior makes comparison with the steady symmetric solution useless. Instead, in this case we validated the numerical model by comparing with the dye spreading during initial development when the flow pattern is still approximately symmetric. The evolution of passive tracer (dye) concentration $\theta(x, y, t)$ was calculated according to

$$\theta_t + J(\psi, \theta) = 0 \quad (56)$$

with the inflow boundary condition

$$\theta(0, y, t) = 1, \quad -L < y < L, \quad (57)$$

as if the tracer were introduced at the opening of the channel $x = 0$. At the initial moment $t = 0$ there is no dye in the basin $\theta(x, y, 0) = 0$. The streamfunction $\psi(x, y, t)$ in (56) is a time-dependent solution of the initial value problem (5), (6) with $\zeta(x, y, 0) = 0$. The tracer evolution equation was solved numerically using third-order upstream differences as in Leonard (1977) generalized to two-dimensions according to Ekebjærg and Justesen (1991). This scheme does not introduce artificial numerical diffusivity, but introduces some higher order dispersion effects.

In the experimental photograph of the dye concentration in Fig. 9a, for example, we superimposed the isoline $\theta = 1/2$ at the appropriate moment in time (dimensional $t = 136 \text{ s}$ from the onset of pumping) calculated according to (56), (57). If the flow were exactly laminar, the dye would stay within this contour. Due to mild temporal variability the pattern within the gyre is distorted. However, there is good agreement in a sense of the position and the shape of the dye front between the gyre and its exterior.

In the photograph in [Fig. 9b](#) showing an asymmetric state that develops at large time we superimposed the streamfunction pattern of the (symmetric) steady solution in the limit of large time. If the development of asymmetry were suppressed, the solution would reach a symmetric steady state and the dye distribution would be restricted within the streamline $\psi = 0$. Such a comparison shows gross agreement in size of the developed gyres despite the symmetry being broken.

The positions of the front of the tracer distribution $X_{[\theta=1/2]}$ and the stagnation point $X_{[u=0]}$ closest to the channel opening along $y = 0$ are shown in [Fig. 10](#) as functions of time as calculated by numerical model. Both curves tend to the same limit for large times as expected. The position of the stagnation point shows large oscillations in the beginning that are caused by Rossby waves propagating in a finite computational domain. The lower envelope of the curve $X_{[u=0]}(t)$ describes the growth of the recirculation. Note that the tracer front position $X_{[\theta=1/2]}(t)$ never overshoots $X_{[u=0]}(t)$, which means that dye spreads eastward monotonically approaching the limit.

Yet for larger $Q = 26 \times 10^{-2} \text{ cm}^2 \text{ s}^{-1}$ ([Fig. 11](#), $\text{Re} = 26$, $\text{Fr} = 4106$, $T_S Q/L^2 = 208$) the jet becomes turbulent: the eddies near the axis become irregular. The numerically calculated streamlines of a steady solution (lower half) and the distribution of tracer (upper half) at the appropriate time moment are shown in [Fig. 11c](#) for qualitative comparison. It is seen that the zonal extent of the gyre in the laboratory experiment is shorter than predicted by the steady solution, which can be attributed to eddies enhancing turbulent diffusivity and lowering the effective Reynolds number. This is in general agreement with the scaling law [\(49\)](#) stating that the zonal extent of the gyre is linearly proportional to the Reynolds number. On the other hand, the meridional extent of the gyre is roughly the same as the one predicted by the steady numerical solution. This once again confirms the scaling law [\(47\)](#) or [\(48\)](#) stating that the meridional extent depends only on the balance between inertia and the β effect and does not depend on the strength of dissipation.

5. Summary and conclusions

We have considered the problem of a recirculation gyre driven by a zonal jet on a β plane. In the limiting case of a *strong* jet, when the structure of the flow depends on the momentum flux rather than on the volume flux of the jet, we derived the asymptotic scaling law [\(47\)–\(49\)](#) for the recirculation gyre. The meridional extent of the gyre depends only on the balance between the inertia of the jet and the opposing β effect, while the zonal extent is linearly proportional to the Reynolds number. The steady numerical solutions confirm the scaling law. A simplified model of the flow as a combination of a jet carrying a positive momentum flux and a homogenized recirculation gyre carrying an opposite amount of momentum flux gives the quantitative constant in the scaling law [\(47\)](#), which is in good agreement with the numerical results. Also the gyre is found to form only when the flow in the channel is supercritical with respect to Rossby waves. Thus the recirculation on the β plane can be regarded as a feature similar to a submerged hydraulic jump: a transition between the supercritical flow within the channel and the subcritical (vanishing) flow in the Sverdrup interior of the basin. The addition of bottom drag has the most pronounced effect on the velocities in the recirculation gyre decreasing its transport; the least susceptible to bottom drag is the meridional scale of the gyre.

Laboratory experiments validate the numerical model. There is quantitative agreement with steady solutions and tracer evolution for low Re when flow is close to laminar. For higher Re laboratory experiments show richer behavior with a strong tendency to asymmetric solutions. A similar tendency is also observed in the numerical solutions of wind-driven double-gyre ocean circulation models ([Cessi and Ierley 1995](#); [Meacham 2000](#)).

It is straightforward to apply the results of the above analysis to the Gulf Stream system. Based on hydrographic data [Fofonoff and Hall \(1983, Table 3\)](#) estimated the advective part of the momentum flux TM for several sections across the Gulf Stream. They found that TM decreases from $89 \times 10^9 \text{ N}$ at 74°W to $25 \times 10^9 \text{ N}$ at 56°W . Substituting the former value (since we need an estimate as far westward as possible) for $J = \text{TM}/(H\rho)$, $H = 5 \text{ km}$ for the depth of the recirculation, and $\beta = 2 \times 10^{-11} \text{ m}^{-1} \text{ s}^{-1}$ into [\(47\)](#) we obtain the meridional scale of the Gulf Stream recirculation $Y_G = 470 \text{ km}$ or 4.2° latitude.

This value is consistent with the direct zonal flow measurements by deep (2000 m and 4000 m) moored current meters and SOFAR floats (at 700 m) at 55°W ([Richardson 1985, Fig. 2a](#)) producing an estimate for Y_G (as a distance from the axis of the jet to the second zero of the zonal velocity) from 3 to 5 degrees of latitude.

Of course, we have to keep in mind the inherent limitations of our simplified model: it ignores the wind-driven circulation in the interior of the subtropical gyre, baroclinic and buoyancy effects, interaction with topography, the role of the deep western boundary current, space- and time-dependent forcing, etc. However, combining all these effects together would preclude any theoretical progress. Specifically, our barotropic vorticity [equation \(5\)](#) is not general since it neglects the vertical stretching term. This can be justified if the scale of the gyre is much larger than the Rossby radius of deformation, $Y_G \ll L_R$. According to [Fofonoff and Hall \(1983\)](#) $L_R = 40 \text{ km}$ in the Gulf Stream area and our assumption is valid.

In this study we deliberately suppressed all eddies in order to more cleanly exhibit steady recirculation gyres. We successfully parameterized the turbulence by the constant viscosity ν because the role of eddies in barotropic recirculation dynamics is simply downgradient diffusion. Eventually, it turned out that certain characteristics of the recirculation gyre, such as Y_G , are independent of ν . This is analogous to other hydraulic problems: the height of a hydraulic jump does not depend on the structure of the turbulent motions behind it.

Acknowledgments

The author is very grateful to Joe Pedlosky for numerous theoretical discussions of the problem, to Larry Armi for discussions of a β -plane hydraulic theory, to Nelson Hogg for discussing observational data, to Jack Whitehead and Karl Helfrich for sharing their expertise in conducting laboratory experiments, and to John Salzig for help in implementing the experimental design. The author would like to thank two anonymous reviewers for their constructive criticism and Barbara Gaffron for proofreading the manuscript. This work was supported by the National Science Foundation through Grant OCE-9810606 and by Woods Hole Oceanographic Institution Endowed funds.

REFERENCES

- Armi L., 1989: Hydraulic control of zonal currents on a β -plane. *J. Fluid Mech.*, **201**, 357–377. [Find this article online](#)
- Batchelor G. K., 1956: On steady laminar flow with closed streamlines at large Reynolds number. *J. Fluid Mech.*, **1**, 177–190. [Find this article online](#)
- Cessi P., and G. R. Ierley, 1995: Symmetry-breaking multiple equilibria in quasi-geostrophic, wind-driven flows. *J. Phys. Oceanogr.*, **25**, 1196–1205. [Find this article online](#)
- Cessi P., and W. R. Young, 1987: A model of the inertial recirculation driven by potential vorticity anomalies. *J. Phys. Oceanogr.*, **17**, 1640–1652. [Find this article online](#)
- Chow V. T., 1959: *Open-Channel Hydraulics*. McGraw-Hill, 680 pp.
- Cummins P. F., 1992: Inertial gyres in decaying and forced geostrophic turbulence. *J. Mar. Res.*, **50**, 545–566. [Find this article online](#)
- Ekebjærg L., and P. Justesen, 1991: An explicit scheme for advection–diffusion modeling in two dimensions. *Comput. Methods Appl. Mech. Eng.*, **88**, 287–297. [Find this article online](#)
- Fischer J., M. Rhein, F. Schott, and L. Stramma, 1996: Deep water masses and transports in the Vema Fracture Zone. *Deep-Sea Res. I*, **43**, 1067–1074. [Find this article online](#)
- Fofonoff N. P., 1954: Steady flow in a frictionless homogeneous ocean. *J. Mar. Res.*, **13**, 254–262. [Find this article online](#)
- Fofonoff N. P., and M. M. Hall, 1983: Estimates of mass, momentum, and kinetic energy fluxes of the Gulf Stream. *J. Phys. Oceanogr.*, **13**, 1868–1877. [Find this article online](#)
- Gradsteyn I. S., and I. M. Ryzhik, 1980: *Tables of Integrals, Series, and Products*. Academic Press, 1160 pp.
- Griffa A., and R. Salmon, 1989: Wind-driven ocean circulation and equilibrium statistical mechanics. *J. Mar. Res.*, **47**, 457–492. [Find this article online](#)
- Henderson F. M., 1966: *Open Channel Flow*. Macmillan, 522 pp.
- Hogg N. G., 1992: On the transport of the Gulf Stream between Cape Hatteras and the Grand Banks. *Deep-Sea Res.*, **39**, 1231–1246. [Find this article online](#)
- Holland W. R., and W. J. Schmitz, 1985: Zonal penetration scale of model midlatitude jets. *J. Phys. Oceanogr.*, **15**, 1859–1875. [Find this article online](#)
- Ierley G. R., 1987: On the onset of inertial recirculation in barotropic general circulation models. *J. Phys. Oceanogr.*, **17**, 2366–2374. [Find this article online](#)
- Ierley G. R., and W. R. Young, 1991: Viscous instabilities in the western boundary layer. *J. Phys. Oceanogr.*, **21**, 1323–1332. [Find this article online](#)
- Ierley G. R., and V. A. Sheremet, 1995: Multiple solutions and advection-dominated flows in the wind-driven circulation. Part I: Slip. *J.*

Jayne S. R., and N. G. Hogg, 1999: On recirculation forced by an unstable jet. *J. Phys. Oceanogr.*, **29**, 2711–2718. [Find this article online](#)

Jayne S. R., and P. Malanotte-Rizzoli, 1996: Recirculation gyres forced by a beta plane jet. *J. Phys. Oceanogr.*, **26**, 492–504. [Find this article online](#)

Kamenkovich V. M., 1966: A contribution to the theory of the inertial–viscous boundary layer in a two-dimensional model of ocean currents. *Izv. Acad. Sci. USSR, Atmos. Oceanic Phys.*, **2**, 781–792, (Translated from Russian.). [Find this article online](#)

Lafuente J. G., N. Cano, M. Vargas, J. P. Rubin, and A. Hernandez-Guerra, 1998: Evolution of the Alboran Sea hydrographic structures during July 1993. *Deep-Sea Res. I*, **45**, 39–65. [Find this article online](#)

Landau L. D., and E. M. Lifshitz, 1959: *Fluid Mechanics*, Pergamon, 536 pp.

Leonard B. P., 1977: A stable and accurate convective modelling procedure based on quadratic upstream interpolation. *Comput. Methods Appl. Mech. Eng.*, **19**, 59–98. [Find this article online](#)

Marshall D., and J. Marshall, 1992: Zonal penetration scale of midlatitude oceanic jets. *J. Phys. Oceanogr.*, **22**, 1018–1032. [Find this article online](#)

McCartney M. S., S. L. Bennett, and M. E. Woodgate-Jones, 1991: Eastward flow through the Mid-Atlantic Ridge at 11°N and its influence on the abyss of the eastern basin. *J. Phys. Oceanogr.*, **21**, 1089–1121. [Find this article online](#)

Meacham S. P., 2000: Low-frequency variability in the wind-driven circulation. *J. Phys. Oceanogr.*, **30**, 269–293. [Find this article online](#)

Nof D., and T. Pichevin, 1999: The establishment of the Tsugaru and the Alboran Gyres. *J. Phys. Oceanogr.*, **29**, 39–54. [Find this article online](#)

Polzin K. L., K. G. Speer, J. M. Toole, and R. W. Schmitt, 1996: Intense mixing of Antarctic Bottom Water in the equatorial Atlantic Ocean. *Nature*, **380**, 54–57. [Find this article online](#)

Preller R. H., 1986: A numerical model study of the Alboran Sea gyre. *Progress in Oceanography*, Vol. 16, Pergamon, 113–146.

Preller R. H., and H. E. Hurlburt, 1982: A reduced gravity numerical model of circulation in the Alboran Sea. *Hydrodynamics of Semi-Enclosed Seas*, J. C. J. Nihoul, Ed., Elsevier Science, 75–90.

Rhines P. B., and W. R. Young, 1982: Homogenization of potential vorticity in planetary gyres. *J. Fluid Mech.*, **122**, 347–367. [Find this article online](#)

Richardson P. L., 1985: Average velocity and transport of the Gulf Stream near 55°W. *J. Mar. Res.*, **43**, 83–111. [Find this article online](#)

Rossby C.-G., 1950: On the dynamics of certain types of blocking waves. *J. Chin. Geophys. Soc.*, **2**, 1–13.

Schlichting H., 1933: Laminare Strahlbreitung. *Z. Angew. Math. Mech.*, **13**, 260. [Find this article online](#)

Schlichting H., 1960: *Boundary Layer Theory*, 4th ed. McGraw-Hill, 647 pp.

Schneider W., 1985: Decay of momentum flux in submerged jets. *J. Fluid Mech.*, **154**, 91–110. [Find this article online](#)

Sheremet V. A., G. R. Ierley, and V. M. Kamenkovich, 1997: Eigenanalysis of the two-dimensional wind-driven ocean circulation problem. *J. Mar. Res.*, **55**, 57–92. [Find this article online](#)

Stern M. E., 1975: Minimal properties of planetary eddies. *J. Mar. Res.*, **33**, 1–13. [Find this article online](#)

Stewartson K., 1957: On almost rigid rotations. *J. Fluid Mech.*, **3**, 17–26. [Find this article online](#)

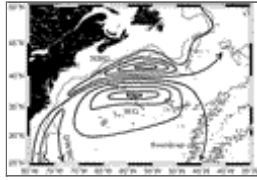
Sverdrup H. U., M. W. Johnson, and R. H. Fleming, 1942: *The Oceans: Their Physics, Chemistry, and General Biology*. Prentice-Hall, 1087 pp.

Taneda S., 1956: Experimental investigation of the wakes behind cylinders and plates at low Reynolds number. *J. Phys. Soc. Japan*, **11**, 302–307. [Find this article online](#)

Worthington L. V., 1976: *On the North Atlantic Circulation, The John Hopkins Oceanographic Studies*, No. 6, The John Hopkins University Press, 110 pp.

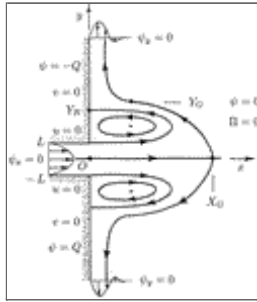
Zauner E., 1985: Visualization of the viscous flow induced by a round jet. *J. Fluid Mech.*, **154**, 111–119. [Find this article online](#)

Figures



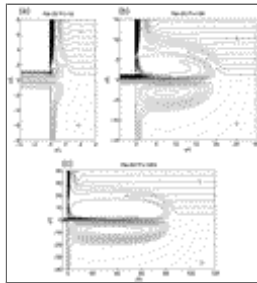
Click on thumbnail for full-sized image.

FIG. 1. Scheme for the recirculation in the Gulf Stream system that is consistent with transport observations made by current meters. Heavy lines are streamlines. To the north of the central jet is the northern recirculation gyre (NRG) carrying 40–60 Sv and to the south of the jet is the Worthington gyre (WG) also carrying 40–60 Sv. DWBC is the deep western boundary current (adapted from [Hogg 1992](#))



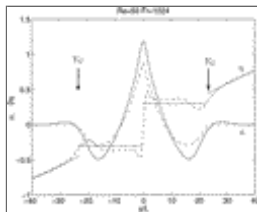
Click on thumbnail for full-sized image.

FIG. 2. Sketch of the problem formulation: a jet entering an infinite basin



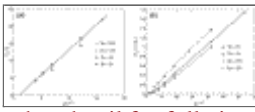
Click on thumbnail for full-sized image.

FIG. 3. Development of the recirculation for fixed $Re = 50$ and increasing Froude–Rossby number Fr . The lower half of each plot shows the streamfunction field ψ while the upper half shows the potential vorticity field $q = \zeta + \beta y$. (a) $Fr = 16$, the contour interval of ψ/Q , $CI_\psi = 0.2$, the contour interval of $q/(Q/L^2)$, $CI_q = 0.5$; (b) $Fr = 128$, $CI_\psi = 0.25$, $CI_q = 0.1$; (c) $Fr = 1024$, $CI_\psi = 0.5$, $CI_q = 0.05$. The dotted lines show the contours of $\psi = 0$ in the region where the flow is weak



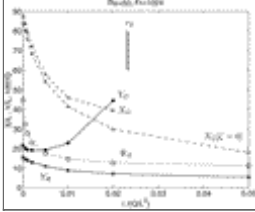
Click on thumbnail for full-sized image.

FIG. 4. Zonal profiles for $Re = 50$, $Fr = 1024$ near the center of the recirculation gyre at $x/L = 34.57$. The solid line is the zonal velocity u divided by Q/L , the dashed line is q divided by $0.5Q/L^2$. The dash–dotted line is the zonal velocity and the dotted line is the potential vorticity according to the homogenized gyre model [\(33\)](#), [\(32\)](#). The vertical lines indicate the theoretical prediction [\(47\)](#) for the meridional extent of the gyre Y_G



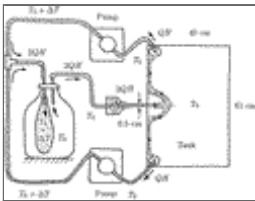
[Click on thumbnail for full-sized image.](#)

FIG. 5a. The dependence of the meridional scale of the gyre Y_G on the Froude–Rossby number Fr . The data for several values of Re are plotted vs $Fr^{2/5}$. The straight solid line represents the theoretical scaling law (48). Fig. 5b. The dependence of the zonal extent of the recirculation gyre X_G divided by LRe on $Fr^{3/5}$. The data for $Re = 20, 50, 100, 200$ are marked in the same way as in (a) but the points for fixed Re are now connected.



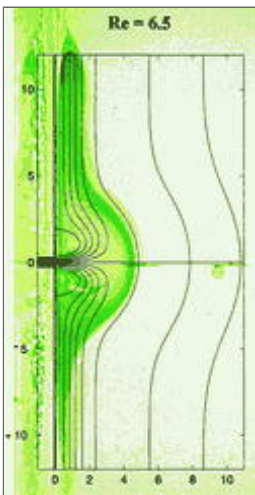
[Click on thumbnail for full-sized image.](#)

FIG. 6. The dependence of the recirculation gyre scales for $Re = 50$ and $Fr = 1024$ on bottom drag r . The spatial scales are nondimensionalized by L , while the gyre transport Ψ_G is nondimensionalized by Q and multiplied by 10



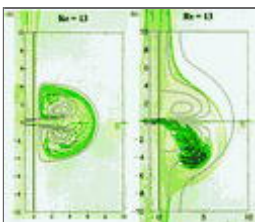
[Click on thumbnail for full-sized image.](#)

FIG. 7. Sketch of the experimental design



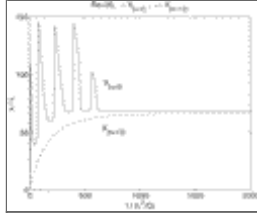
[Click on thumbnail for full-sized image.](#)

FIG. 8. A photograph of the dye spreading in the laboratory experiment with $Re = 6.5$, $Fr = 1026$, $T_S Q/L^2 = 52$ with streamlines of the steady numerical solution superimposed. At this moment (8 min from the start of pumping) the gyre has already reached the equilibrium extent, while the distribution of dye within the western boundary layers is still developing. The horizontal scales are in cm



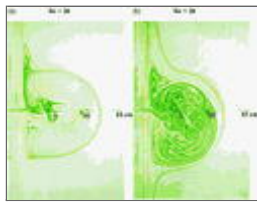
[Click on thumbnail for full-sized image.](#)

FIG. 9. Two photographs illustrating the development of the gyre and spreading of dyed fluid in the experiment with $Re = 13$, $Fr = 2053$, $T_S Q/L^2 = 104$: (a) $t = 136$ s (from the start of pumping), the two gyres are still symmetric with a mild degree of instability of the jet. Superimposed is the contour $\theta = 1/2$ of the passive tracer distribution. Ideally all the dyed fluid should be confined by it. (b) $t = 525$ s, a quasi-steady asymmetric state with the southern gyre dominating the northern one: a puff of newly introduced dyed fluid reveals the deflection of the jet south. Superimposed are the streamlines of the symmetric limiting steady solution. The contour interval is $Q/2$. The horizontal scales are in cm



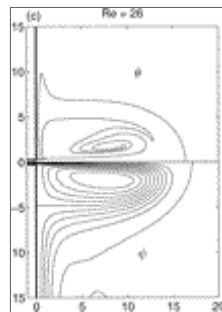
[Click on thumbnail for full-sized image.](#)

FIG. 10. Plots of two different measures defining the zonal extent of the recirculation gyre: the stagnation point of the velocity field $X_{[u=0]}$ (solid line) and the position of the front of the dyed fluid $X_{\theta=1/2}$ (dashed line) versus time for the experiment with $Re = 26$, $Fr = 4106$, $T_S Q/L^2 = 208$.



[Click on thumbnail for full-sized image.](#)

FIG. 11. The experiment with $Re = 26$, $Fr = 4106$, $T_S Q/L^2 = 208$. (a) A photograph of two quasi-symmetric recirculation gyres at $t = 10$ min (from the start of pumping); the jet is wildly unstable. (b) A photograph of an asymmetric flow at $t = 15$ min. (c) The numerically calculated stream function of the corresponding limiting symmetric steady solution (lower half, the contour interval $Q/5$) and the contour $\theta = 1/2$ of the passive tracer distribution at $t = 1000L^2/Q = 4$ min (upper half). The horizontal scales are in cm



[Click on thumbnail for full-sized image.](#)

FIG. 11. (Continued)

* Woods Hole Oceanographic Institution Contribution Number 10373.

Corresponding author address: Dr. Vitalii A. Sheremet, Woods Hole Oceanographic Institution, MS #21, Woods Hole, MA 02543. E-mail: vsheremet@whoi.edu



© 2008 American Meteorological Society [Privacy Policy and Disclaimer](#)

Headquarters: 45 Beacon Street Boston, MA 02108-3693

DC Office: 1120 G Street, NW, Suite 800 Washington DC, 20005-3826

amsinfo@ametsoc.org Phone: 617-227-2425 Fax: 617-742-8718

[Allen Press, Inc.](#) assists in the online publication of *AMS* journals.